Assessment of Ovarian Tumor Growth in Wild-Type and Lumican-Deficient Mice: Insights Using Infrared Spectral Imaging, Histopathology, and Immunohistochemistry

Pierre Nizet, Valérie Untereiner, Ganesh D Sockalingum, Isabelle Proult, Christine Terryn, Albin Jeanne, Lise Nannan, Camille Boulagnon-Rombi, Christèle Sellier, Romain Rivet, et al.

Assessment of Ovarian Tumor Growth in Wild-Type and Lumican-Deficient Mice: Insights Using Infrared Spectral Imaging, Histopathology, and Immunohistochemistry

Pierre Nizet[1,2], Valérie Untereiner[3], Ganesh D. Sockalingum[4,*], Isabelle Proult[1,2], Christine Terryn[3], Albin Jeanne[5], Lise Nannan[1,2], Camille Boulagnon-Rombi[2,6], Christèle Sellier[1,2], Romain Rivet[1,2], Laurent Ramont[1,2,7], and Stéphane Brézillon[1,2,*].

[1] Laboratoire de Biochimie Médicale et Biologie Moléculaire, Université de Reims Champagne-Ardenne, 51097 Reims, France; [2] CNRS UMR 7369, Matrice Extracellulaire et Dynamique Cellulaire-MEDyC, 51097 Reims, France; [3] PICT, Université de Reims Champagne-Ardenne, 51097 Reims, France; [4] BioSpec*T*-EA7506, Université de Reims Champagne-Ardenne, 51097 Reims, France; [5] Apmonia Therapeutics, 51686 Reims, France; [6] CHU Reims, Service de Pathologie, Université de Reims Champagne-Ardenne, 51097 Reims, France; [7] CHU Reims, Service Biochimie-Pharmacologie-Toxicologie, 51097 Reims, France; * Correspondence: ganesh.sockalingum@univ-reims.fr (G.D.S.), stephane.brezillon@univ-reims.fr (S.B.)

ABSTRACT

Ovarian cancer remains one of the most fatal cancers because of lack of robust screening methods of detection at early stages. **Extracellular matrix (ECM)** mediates interactions between cancer cells and their microenvironment *via* specific molecules. **Lumican**, a small leucine-rich proteoglycan (SLRP), maintains ECM integrity and inhibits both melanoma primary tumor development and metastatic spreading. **The aim of this study was to analyze the effect of lumican on tumor growth of murine ovarian epithelial carcinoma.** C57BL/6 wild type mice (n=12) and lumican-deficient mice (n=10) were subcutaneously injected with murine ovarian epithelial carcinoma ID8 cells and sacrificed after 18 days. Analysis of tumor volumes demonstrated an inhibitory effect of endogenous lumican on ovarian tumor growth. The ovarian primary tumors were subjected to **histological and immunohistochemical staining** using anti-lumican, anti-αv integrin, anti-CD31 and anti-cyclin D1 antibodies, and further examined by **label-free infrared spectral imaging** (IRSI), **second harmonic generation** (SHG) and **Picrosirius Red** staining. The IR tissue images identified different ECM tissue regions of the skin and the ovarian tumor. Moreover, IRSI showed a good correlation of αv integrin immunostaining and collagen organization within the tumor. Our results demonstrate for the first time that lumican inhibits the growth of ovarian cancer mainly by altering collagen organization and distribution.

WORKFLOW AT A GLANCE

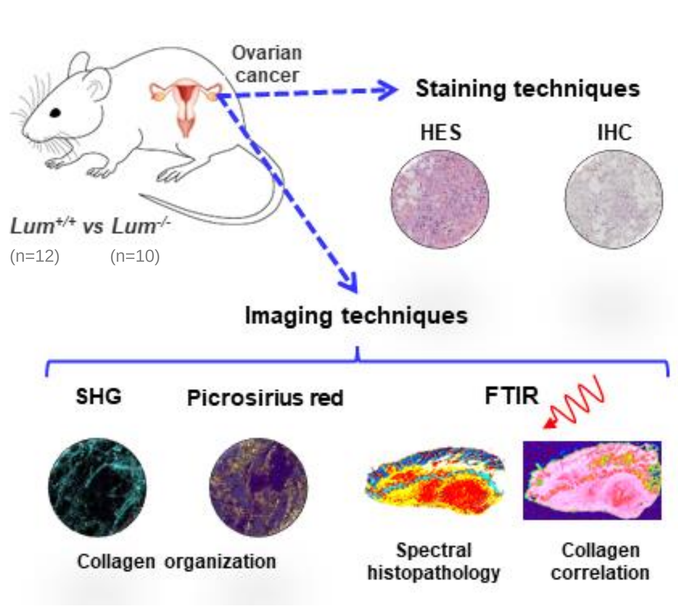

FIGURE 1

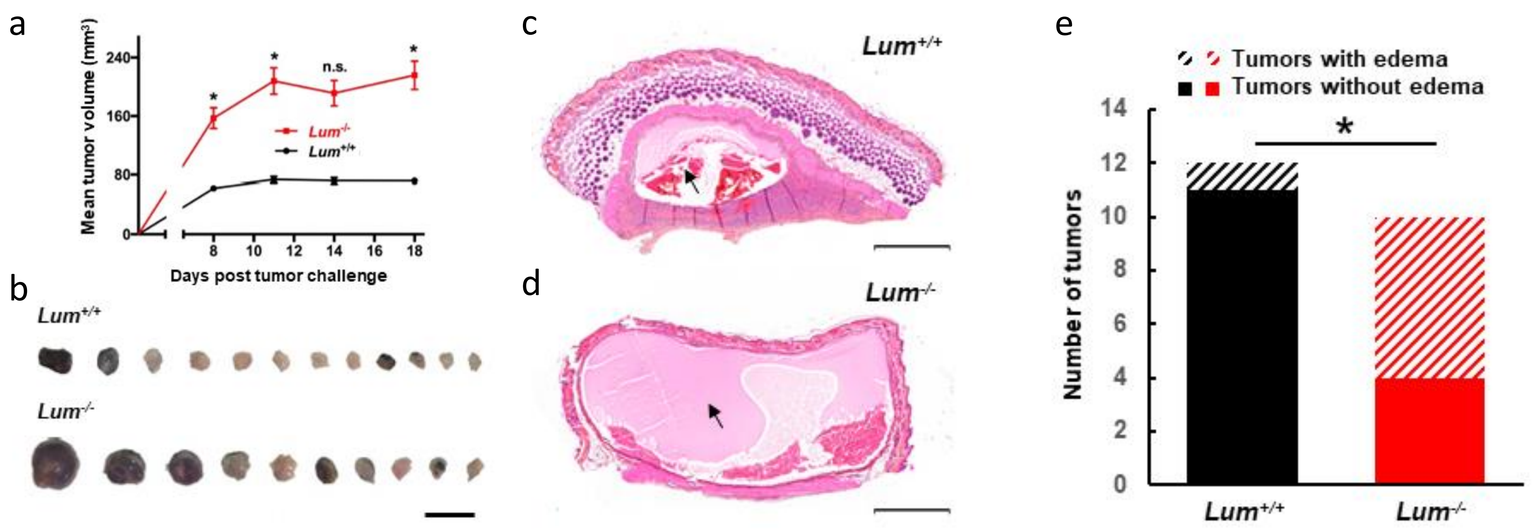

Evaluation of endogenous lumican impact on tumor growth in an ovarian allograft model. (**a-b**) ID8 ovarian tumor cells (2.5 x 10^5) were s.c. inoculated in wild-type (*Lum*$^{+/+}$) or lumican-deficient (Lum$^{-/-}$) syngeneic C57BL/6J mice; (**a**) Averages of calculated tumor volumes in mm^3 (mean ± SEM, n = 10–12 per group) (*t* test, ns not significant, *p < 0.05); (**b**) Representative photographs of ID8 ovarian tumors s.c. allografts after tumor excision (scale bar, 1 cm). Representative images of edemas observed in HES staining of *Lum*$^{+/+}$ (**c**) and *Lum*$^{-/-}$ (**d**) tumor sections are shown (scale bar, 500 µm); (**e**) Quantification of the number of edemas observed in ovarian tumor sections of *Lum*$^{+/+}$ or *Lum*$^{-/-}$ syngeneic C57BL/6J mice (*p < 0.05).

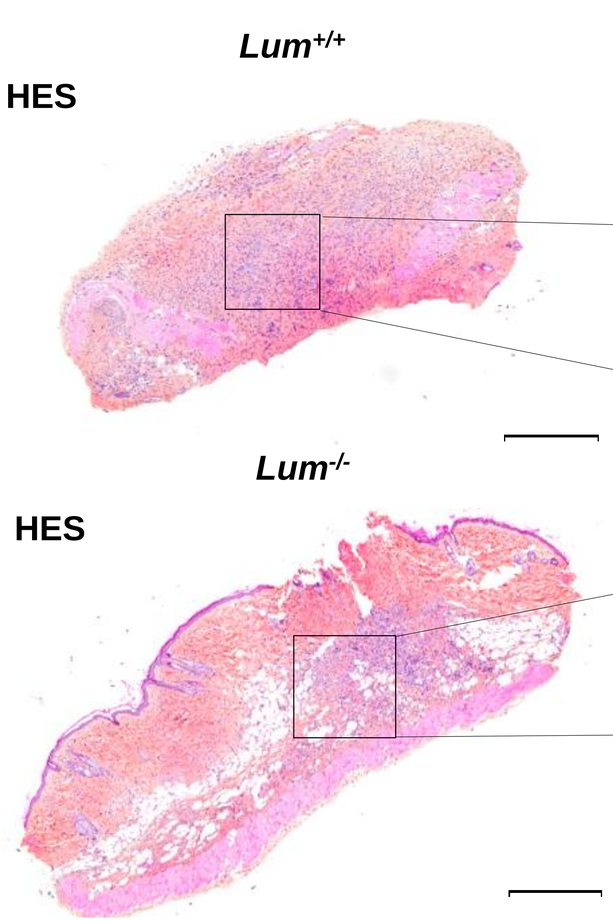

Example of s.c. allograft whole sections stained with HES (scale bar 500 µm) in wild-type (*Lum*$^{+/+}$, top) and lumican-deficient (*Lum*$^{-/-}$, bottom) mice.

FIGURE 2

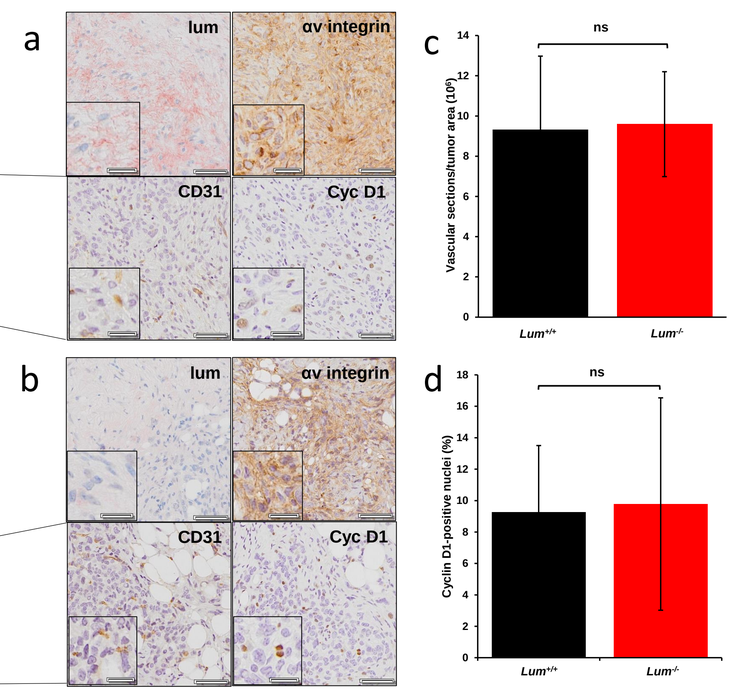

Histological and immunohistochemical analysis of ovarian tumor sections. (**a, b**) IHC analyses of ovarian allografts in tumors implanted in *Lum*$^{+/+}$ (**a**) and *Lum*$^{-/-}$ (**b**) mice, Microscopic views of s.c. allograft whole sections IHC allowing visualization of lumican, αv integrin, CD31 and cyclin D1 (scale bar 50 µm); (**c, d**) Quantification of percentage of CD31-positive blood vessels (**c**) as well as relative cyclin D1-positive areas (number of positive cyclin D1 tumor cell nuclei normalized to the total number of tumor cell nuclei) (**d**) (mean ± standard deviation, Mann-Whitney U test, ns not significant). Insets are showing higher magnification (scale bar 20 µm). All acquisitions were performed with a 20x magnification.

FIGURE 3

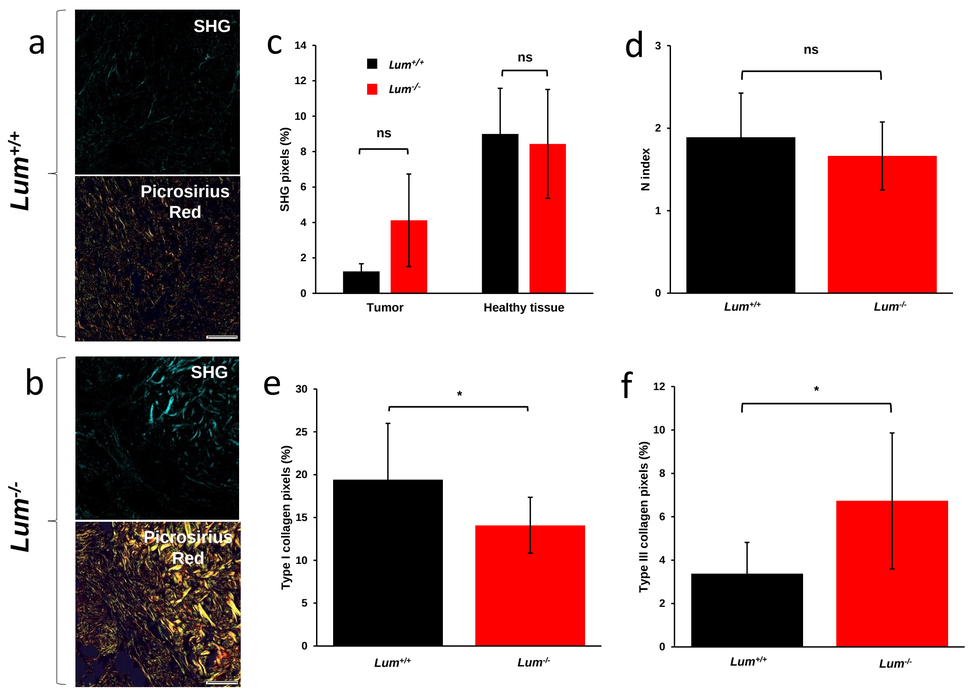

Analysis of collagen organization in ovarian tumor sections of wild-type and lumican-deficient mice. (**a, b**) SHG image analyses and Picrosirius red staining (viewed under widefield cross-polar optics) of ovarian allografts in tumors implanted in *Lum*$^{+/+}$ mice (**a**) and in tumors from *Lum*$^{-/-}$ mice (**b**) (scale bar 50 µm, original magnification 20x); (**c**) Analysis of collagen fibers intensity by SHG in tumors and healthy tissues present in each section (mean ± standard deviation, Mann-Whitney U test, ns not significant); (**d**) Analysis of tumor ECM collagen organization from images derived from Gabor filtering and FFT, processed on Picrosirius red images (mean ± standard deviation, Mann-Whitney U test, ns not significant); (**e**) Quantification on Picrosirius red stained sections of the relative distribution of red pixels (corresponding to type I collagen) in tumor ECM of Lum$^{+/+}$ and Lum$^{-/-}$ sections (mean ± standard deviation, Mann-Whitney U test, * p < 0.05); (**f**) Quantification on Picrosirius red stained sections of the relative distribution of green pixels (corresponding to type III collagen) within tumors of Lum$^{+/+}$ and Lum$^{-/-}$ sections (mean ± standard deviation, Mann-Whitney U test, * p < 0.05).

FIGURE 4

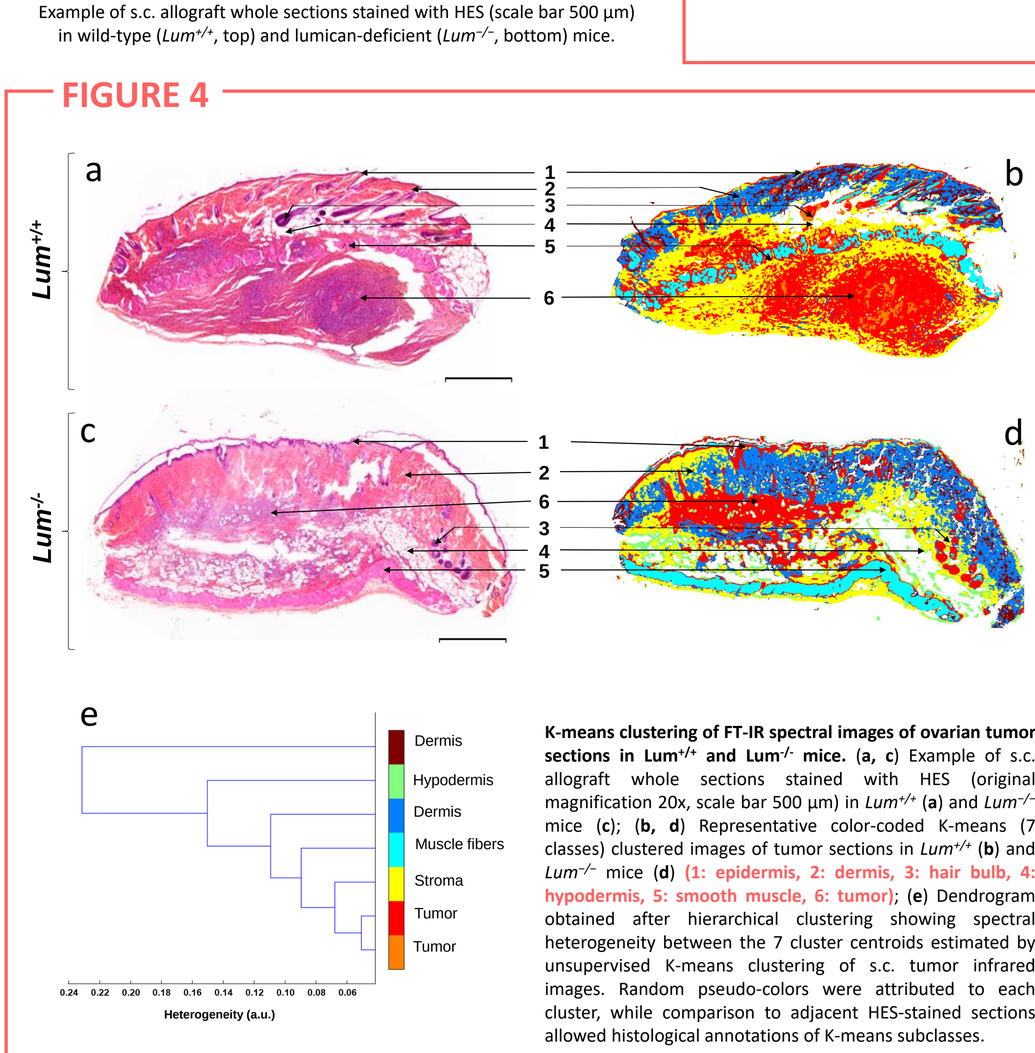

K-means clustering of FT-IR spectral images of ovarian tumor sections in Lum$^{+/+}$ and Lum$^{-/-}$ mice. (**a, c**) Example of s.c. allograft whole sections stained with HES (original magnification 20x, scale bar 500 µm) in *Lum*$^{+/+}$ (**a**) and *Lum*$^{-/-}$ mice (**c**); (**b, d**) Representative color-coded K-means (7 classes) clustered images of tumor sections in *Lum*$^{+/+}$ (**b**) and *Lum*$^{-/-}$ mice (**d**) (1: epidermis, 2: dermis, 3: hair bulb, 4: hypodermis, 5: smooth muscle, 6: tumor); (**e**) Dendrogram obtained after hierarchical clustering showing spectral heterogeneity between the 7 cluster centroids estimated by unsupervised K-means clustering of s.c. tumor infrared images. Random pseudo-colors were attributed to each cluster, while comparison to adjacent HES-stained sections allowed histological annotations of K-means subclasses.

FIGURE 5

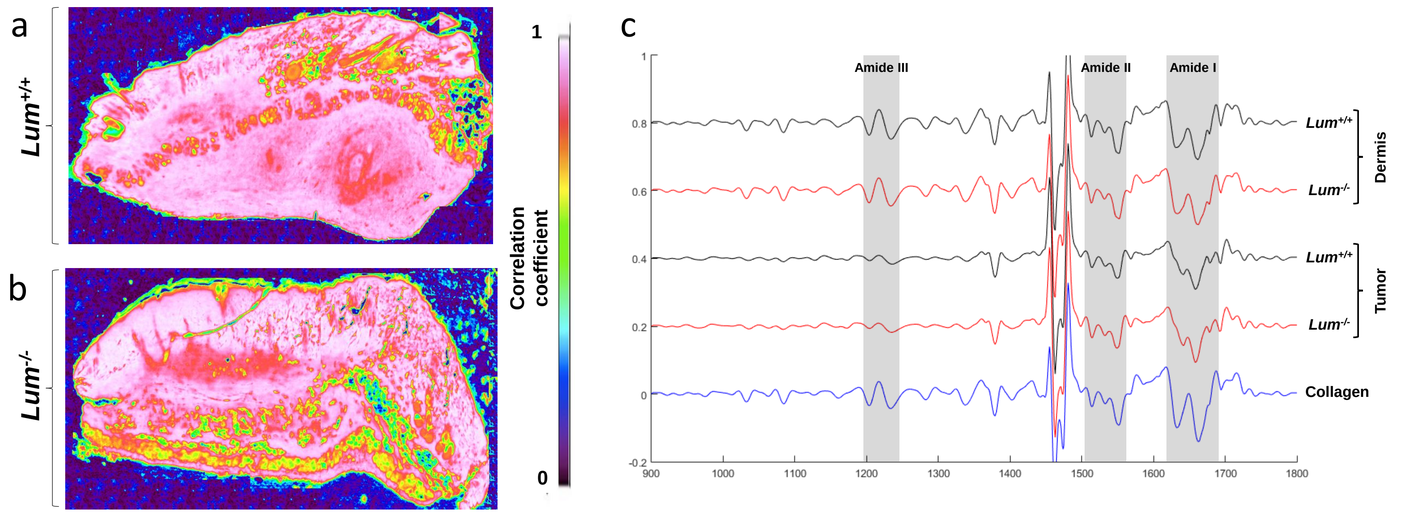

Correlation maps using type I collagen reference spectrum. (**a, b**) Type I collagen correlation images of Lum$^{+/+}$ (**a**) and Lum$^{-/-}$ (**b**) spectral images (scale bar 500 µm). The latter were each correlated with a pure type I collagen spectrum. Provided scale indicates the degree of correlation from 0 (black, not correlated) to 1 (white, totally correlated). (**c**) Comparison between type I collagen second-derivative spectrum (blue line) with second-derivative spectra taken randomly from the dermis and tumors of Lum$^{+/+}$ (black lines) and Lum$^{-/-}$ (red lines) mice skin tissues. Second-derivative spectra are offset for clarity. The corresponding bands of Amide I, II and III, as well as collagen-characteristic zones are highlighted.

CONCLUSIONS

Overall, our findings are the first to highlight the major role of lumican in the maintenance of the extracellular matrix integrity in the context of ovarian cancer, showing its inhibitory role in primary ovarian tumor growth. Thanks to a multimodal approach, combining histopathology, immunohistochemistry and imaging techniques, the alteration of collagen organization could be demonstrated in tumors from lumican-deficient mice. This disorganization was associated with a significant increase in tumor growth and edema formation within the tumors. Non-invasive methods such as vibrational spectroscopy might be promising diagnostic techniques for ovarian tumor detection at early stages.

Funding: The Université de Reims Champagne-Ardenne is gratefully acknowledged for funding of P.N.'s PhD thesis. This research was also funded by SFR Cap Santé as part of the ISOVALUM project. **Institutional Review Board Statement**: All mice procedures were conformed to the ethical rules of the University of Reims Champagne-Ardenne ethics committee (n°C2EA-56) and were approved by the URCA animal facility platform (URCAnim, Reims, EU0362) and the CNRS. This study was performed respecting "The French Animal Welfare Act" and "The French Board for Animal Experiments". Experiments were conducted under approval of the French "Ministère de l'Enseignement Supérieur et de la Recherche" in compliance with the "Directive 2010/63/UE", protocol number: APAFIS#02206.02, February 2016). **Acknowledgements:** we would like to thank Pr. Shukti Chakravarti for providing the heterozygous lumican-deficient mice, and the URCA-PICT platform for all the equipment used for imaging and spectroscopy. We are also thankful to Dr. Cyril Gobinet for script development in MATLAB software, and the URCAnim platform (P. Lecuivre and A. Pigeon) for animal care.